

Elongation effect on beta-induced Alfvén eigenmode

Gengxian Li¹, Yueyan Li² and Yong Xiao^{1,*} 

¹ Institute for Fusion Theory and Simulation, Zhejiang University, Hangzhou, 310027, China

² National Supercomputing Center of Tianjin, China

E-mail: yxiao@zju.edu.cn

Received 27 August 2022, revised 19 October 2022

Accepted for publication 15 November 2022

Published 2 December 2022



CrossMark

Abstract

Beta induced Alfvén eigenmode (BAE) can be an important candidate for ion loss in burning plasmas. Elongation effect on BAE has been investigated by the gyrokinetic eigenvalue code DAEPS in this work. We construct a shaped equilibrium model by modifying local $s - \alpha$ model with which the capability of the DAEPS code has been extended to study the elongation effect. It is discovered that the BAE growth rate first increases with elongation factor κ , reaches a maximum and then decreases. This trend occurs for many different values of η_i . We find that, in the weak or moderate elongation region, the BAE instability is reactive type and mainly determined by the fluid/MHD effects, namely the combination of stabilizing field line bending term and destabilizing interchange drive in the vorticity equation. However, in the strong elongation region, the BAE instability becomes dissipative and is mainly driven by the wave–particle resonance effect embedded in δW_k since the fluid driving damps away. It is also discovered that the wave–particle resonance decreases with elongation in this region, which is due to the decrease of the geodesic curvature with elongation and leads to the decrease in the growth rate of BAE.

Keywords: elongation, Alfvén eigenmodes, shaping effect

(Some figures may appear in colour only in the online journal)

1. Introduction

Energetic particles (EPs) can destabilize various Alfvénic instabilities, which in turn can substantially degrade the confinement for the EPs. The common Alfvénic instabilities include toroidicity induced Alfvén eigenmode [1–5], beta induced Alfvén eigenmode (BAE) [6–12], EP mode [13–15], reversed shear Alfvén eigenmode (RSAE) [16, 17], etc. Among them, BAE has a characteristic frequency below the shear Alfvén continuous spectrum in the beta-induced gap, which is caused by the coupling between the shear Alfvén wave (SAW) and ion sound wave (SW). BAE could lead to a major ion loss in fusion device, and it can be destabilized by

either EPs or thermal ions. The BAE mode has been observed by DIII-D tokamak experiments, where an Alfvénic instability with the BAE frequency is excited by neutral beam injection only in high beta plasmas [18]. Progress has been made in theory and simulation of the BAE mode during the last two decades [8, 19]. For example, with the asymptotic matching method, an analytic theory has been developed to investigate the BAE linear instability based the $s - \alpha$ model with concircular magnetic fluxes [20]. Recently both fluid-kinetic hybrid simulation and gyrokinetic simulation have been developed to looked into the linear and nonlinear BAE physics [6, 21–24], e.g., wave–particle trapping has been recently discovered to be the main saturation mechanism of BAE turbulence [24]. Here we employ a newly developed non-perturbative linear eigenvalue code named DAEPS [25] (drift Alfvén EP stability) to investigate the plasma shaping effect on the BAE instability.

The DAEPS code is based on the general fishbone-like dispersion relation (GFLDR) theoretical framework and uses the

* Author to whom any correspondence should be addressed.



Original content from this work may be used under the terms of the [Creative Commons Attribution 4.0 licence](https://creativecommons.org/licenses/by/4.0/). Any further distribution of this work must maintain attribution to the author(s) and the title of the work, journal citation and DOI.

numerical method of finite element to calculate various unstable or stable drift Alfvénic eigenmodes in toroidal plasmas [25]. This code uses an iteration method to solve the vorticity equation, as well as to obtain the complex frequency ω and asymptotic behaviour Λ with high precision. In addition, it has used the Neumann boundary condition for accurate asymptotic wave behaviour in the inertial region of the ballooning space, i.e., $\partial_\theta \Psi = i\Lambda \Psi$. Furthermore, in order to speed up numerical integration, a reduced method based on drift center transformation has been developed in DAEPS to calculate the BAE stability [25]. Many numerical codes have investigated the AE physics by setting the perturbed magnetic potential $\Psi = 0$ as the boundary condition [26, 27], which cannot accurately compute the asymptotic mode behaviour and then the eigen frequency on many occasions, especially for those damped modes or marginally unstable modes.

Most previous studies on the AEs are based on a model equilibrium with concircular magnetic flux surface [20, 25]. However, the cross section of magnetic flux surface is generally not circular in modern tokamaks. The plasma shaping factors could be crucial for determining linear instability and nonlinear transport [28]. Therefore, it is important to take plasma shaping factors such as elongation and triangularity into account, which could be a difficult task for the conventional theory [29]. For the model equilibrium, Miller *et al* have used nine parameters to establish an analytic equilibrium for the D-shaped plasma [30]. Here we develop a shaped equilibrium model by following Miller's approach but only focus on the elongation factor. In this equilibrium, an analytical constrain has been found for important physical quantities such as Shafranov shift Δ , elongation factor κ and normalized pressure gradient α . Then we implement this model in the DAEPS code to investigate the elongation effect on the BAE instability. The vorticity equation including the crucial kinetic compression term has been modified to including the elongation factor. It is discovered that the linear growth rate of BAE first increases and then decreases with elongation factor κ . And then how the MHD and kinetic effects together affect the instability of BAE has also been analyzed and discussed in detail.

This paper is organized as follows. In section 2, we show the governing equations in the ballooning representation for the most general magnetic equilibrium. Then we introduce a new equilibrium model with elongation factor κ and demonstrate how the governing equations for drift Alfvénic instabilities are modified by the elongation, where it is crucial to calculate the specific forms for the factors of κ and g in governing equations and implement them in the DAEPS code. Next, section 3 presents numerical results by the DAEPS code, where we exhibit the relationship between the elongation and the growth rate of BAE in various situations. In section 4, we analyze how the elongation affects the BAE instability and make physics interpretations for the numerical results. In section 5, we give a summary for the elongation effect on BAE mode and discuss the future work.

2. Theoretical model

2.1. Vorticity equation and gyrokinetic equation

It has been known that the high- n drift-Alfvénic modes are most relevant for electromagnetic turbulence in large size fusion devices such as ITER. Ballooning representation is conveniently employed here to reduce the complexity of calculating these high- n modes. In order to accurately address the complex magnetic geometry in a tokamak, a particular set of magnetic coordinates, i.e., the Boozer coordinates $(\psi_p, \theta_B, \zeta_B)$ are used in the theoretical modelling and numeric calculation in this paper. The vorticity equation using the ballooning representation and the Boozer coordinates can be written as [14, 25]

$$\begin{aligned} & \partial_\theta \kappa_\perp^2 \partial_\theta \delta\psi + \frac{1}{P_\parallel^2} \frac{\omega(\omega - \omega_{*pi})}{\omega_A^2} \kappa_\perp^2 \delta\psi + \frac{1}{P_\parallel^2} \alpha g \delta\psi \\ & = \sum_j \left\langle \frac{4\pi q_j q^2 R^2}{k_\theta^2 c^2 P_\parallel^2} J_0(k_\perp \rho_j) \omega \omega_{dj} \delta K_j \right\rangle_v. \end{aligned} \quad (1)$$

In the preceding equation, $\partial_\parallel = \frac{P_\parallel}{qR} \partial_\theta$, $P_\parallel = \frac{\kappa B_A r R}{J_B B}$, and θ is the extended poloidal angle in the ballooning representation, $\kappa_\perp = \frac{k_\perp}{k_\theta}$ with $k_\theta = \frac{nq}{r}$, $\omega_A = \frac{v_A}{qR}$ is Alfvén frequency, $\omega_{*pi} = \frac{k \times b}{\Omega_{ci} m_i} \cdot \nabla p_i$ is the ion diamagnetic frequency with Ω_{ci} the ion cyclotron frequency, $\alpha = -Rq^2 \beta'$ with $\beta = 8\pi p_i / B^2$, $\langle \dots \rangle_v \equiv \int \dots d^3v$ is the integration over velocity space, q_j is the charge for the particle species j , $J_0(k_\perp \rho_j)$ is the zeroth order first kind Bessel function with $\rho_j = \frac{v_j}{\Omega_{cj}}$ the Larmor radius, and $\omega_{dj} = \mathbf{k} \cdot \mathbf{b} \times (\mu B + v_\parallel^2) \nabla B / \Omega_{cj}$ is the drift frequency for the particle species j . We further note that the left-hand side of the preceding equation is due to fluid contribution, including field line bending term $\partial_\theta \kappa_\perp^2 \partial_\theta \delta\psi$, inertial term $\frac{1}{P_\parallel^2} \frac{\omega(\omega - \omega_{*pi})}{\omega_A^2} \kappa_\perp^2 \delta\psi$ and ballooning interchange term $\frac{1}{P_\parallel^2} \alpha g \delta\psi$. The right-hand side is due to kinetic compression (KC) of plasmas, which could come from EPs or thermal particles.

The gyrocenter distribution function δK_j could be acquired by solving the linearized collisionless electromagnetic gyrokinetic equation:

$$\left(\frac{P_\parallel}{qR} \partial_\theta - i\omega + i\omega_d \right) \delta K_j = i \frac{q_j}{m_j} Q F_{0j} \frac{\omega_{dj}}{\omega} J_0(k_\perp \rho_j) \delta\psi, \quad (2)$$

where $Q F_{0j} = (\omega \partial_E + \hat{\omega}_{*j}) F_{0j}$ is free energy provided by the phase space gradient of the equilibrium distribution function F_{0j} , with $E = \frac{1}{2} v^2$ and $\hat{\omega}_{*j} = \frac{k \times b}{\Omega_{cj}} \cdot \nabla \ln F_{0j}$.

In the ballooning representation, the vorticity equation of equation (1) can be further organized as a Schrödinger-like form

$$\begin{aligned} & \left[\partial_\theta^2 + \frac{1}{P_\parallel^2} \frac{\omega(\omega - \omega_{*pi})}{\omega_A^2} + V(\theta) \right] \Psi \\ & = \sum_j \left\langle \frac{4\pi q_j}{k_\theta^2 c^2 P_\parallel^2 \kappa_\perp} J_0(k_\perp \rho_j) \omega \omega_{dj} \delta K_j \right\rangle_v, \end{aligned} \quad (3)$$

where $V(\theta) = \frac{1}{P_{\parallel}^2} \frac{\alpha g}{\kappa_{\perp}^2} - \frac{1}{\kappa_{\perp}} \frac{\partial^2 \kappa}{\partial \theta^2}$ is the effective potential well and $\Psi = \kappa_{\perp} \delta \psi$. To calculate accurately the eigen frequency ω of the preceding equation, we need to properly deal with the asymptotic boundary condition in the inertial regime where the parallel coordinate $\theta \gg 1$. The generalized form of the asymptotic vorticity equation can be written as

$$(\partial_{\theta}^2 + \Lambda^2)\Psi = 0 \quad (4)$$

The asymptotic behaviour of Ψ can be derived by the Floquet theory as $\theta \gg 1$:

$$\lim_{\theta \rightarrow \infty} \Psi = P(\theta)e^{i\nu|\theta|}, \quad (5)$$

In the inertial region, the potential well could be divided into a DC component independent of the ballooning angle and an AC component changing with the ballooning angle. With elongation the AC component can no longer be ignored compared to the DC component. Thus $P(\theta)$ is a fast oscillating function with 2π periodicity and $\Lambda = -i\frac{1}{P} \frac{\partial P}{\partial \theta} + \nu$ is the inertial term in the GFLDR theory [31, 32].

The kinetic compression term of equation (3) involves a multi-dimensional integral for δK_j , which can be solved by the gyrokinetic equation equation (2). For studying BAE instability, as the mode frequency in the range of ion transit frequency, the bounce motion of trapped ions can be ignored for the analysis and all particles can be regarded as circulating particles. Thus the gyrokinetic equation can be integrated directly in the ballooning space:

$$\begin{aligned} \delta K_j(\theta, \hat{\sigma}, \lambda, E) &= \hat{\sigma} \int_{-\hat{\sigma}\infty}^{\theta} \exp \left[i\hat{\sigma} \text{sign}(Im\omega) \int_{\theta}^x \frac{-\omega + \omega_{dj}}{P_{\parallel}|v_{\parallel}|} dx \right] \\ &\times i \frac{q_j}{m_j} \frac{qR}{|v_{\parallel}|P_{\parallel}} QF_{0j} \frac{\omega_{dj}(x)}{\omega} J_0 \frac{\Psi(x)}{\kappa_{\perp}(x)} dx \end{aligned} \quad (6)$$

where $\hat{\sigma} = \frac{v_{\parallel}}{|v_{\parallel}|} = \pm 1$ represents co- and counter-direction for the parallel velocity, $\lambda = \frac{\mu B_0}{E}$ is the pitch angle variable. Hence, the kinetic compression term has the following integral form:

$$\begin{aligned} KC &\equiv \kappa_{\perp}^{-1} \left\langle \frac{4\pi q_j q^2 R^2}{k_{\theta}^2 c^2 P_{\parallel}} J_0(k_{\perp} \rho_j) \omega \omega_{dj} \delta K_j \right\rangle_v \\ &= \frac{4\pi q_j q^2 R^2}{k_{\theta}^2 c^2 P_{\parallel}^2} \times \int_0^{+\infty} dE \int_0^1 d\lambda \int_{-\infty}^{+\infty} dx \frac{2\pi E \omega_{dj}(\theta)}{|v_{\parallel}| \kappa_{\perp}(\theta)} J_0 i \frac{q_j}{m_j} \\ &\times \frac{qR}{|v_{\parallel}|P_{\parallel}} QF_{0j} \times \exp \left[i \text{sign}(Im\omega(\theta - x)) \int_{\theta}^x dx qR \right. \\ &\left. \times \frac{-\omega + \omega_{dj}(x)}{|v_{\parallel}|P_{\parallel}} \right] \frac{\omega_{dj}(x)}{\kappa_{\perp}(x)} J_0 \Psi(x) \end{aligned} \quad (7)$$

The computational model for the DAEPS code consists of equations (3), (5) and (7) for the purpose of calculating BAE, which is suitable for arbitrary equilibrium magnetic field. The original DAEPS code is based on a simplify equilibrium field model with concircular cross section. In this paper, we modify the original equilibrium to incorporate the important shaping

factor of elongation by updating geometric coefficients such as κ_{\perp} and g functions in the model equations. The shaped equilibrium magnetic field model is introduced in the following section.

2.2. Equilibrium model with elongation

In order to study the elongation effect on the BAE instability in a tokamak, a local large aspect-ratio plasma equilibrium with shifted elongated flux surfaces is used in this paper. These elongated flux surfaces can be defined by the following equations for their (R, Z) coordinates:

$$\begin{cases} R = 1 + r \cos \theta_g - \Delta(r) \\ Z = \kappa r \sin \theta_g \end{cases} \quad (8)$$

where κ is the elongation factor, θ_g is the geometric poloidal angle, r is a radial variable and a flux label and the length are normalized by major radius R_0 . This model equilibrium is similar to the Miller equilibrium, and includes Shafranov shift $\Delta(r)$. In this model, the flux surface is defined by the radial variable r and the magnetic flux surfaces for different values of elongation are exhibited in figure 1.

The magnetic field associated with this equilibrium model is of the form

$$\mathbf{B} = B_a \nabla \zeta_g + B_a \frac{\kappa r}{q} \nabla \zeta_g \times \nabla r \quad (9)$$

where ζ_g is the geometric toroidal angle, B_a is the on-axis magnetic field.

To the order of $O(r)$, the Jacobian $J_g = (\nabla r_g \cdot \nabla \theta_g \times \nabla \zeta_g)^{-1}$ could be calculated as

$$J_g = \kappa r R (1 - \Delta' \cos \theta_g) \quad (10)$$

In the DAEPS code, the normalized pressure gradient $\alpha = -q^2 \frac{2\mu_0 p'}{B_0^2}$ are actually used to calculate linear instability instead of the Shafranov shift $\Delta(r)$. Thus, we proceed to discuss the relationship between the physical quantities (α, Δ) and the physical quantities (s, α) in the conventional $s - \alpha$ model. For this purpose, we resort to the original Grad–Shafranov (G–S) equation.

$$\nabla \cdot \left(\frac{\nabla \psi_p}{R^2} \right) = -\mu_0 \frac{dP}{d\psi_p} - \frac{F}{R^2} \frac{dF}{d\psi_p}, \quad (11)$$

where $F = B_{\phi} R$ represents the poloidal current. In the $s - \alpha$ model for circular flux surfaces, we can solve this preceding equation by perturbation method according to the smallness of r/R_0 . To the lowest order, the preceding G–S equation can be turned into the following radial force balance equation [33]:

$$2\mu_0 \frac{P'}{B_0^2} + \frac{1}{q^2} \left[\left(3 - 2 \frac{q'r}{q} \right) \Delta' - r + r \Delta'' \right] = 0 \quad (12)$$

From equation (12), ignoring the $O(r)$ term, we can find the relationship between the normalized pressure gradient α and Shafranov shift $\Delta(r)$: $r(\Delta' + r) = \alpha$. However, when the elongation effect is considered, there will be extra shaping

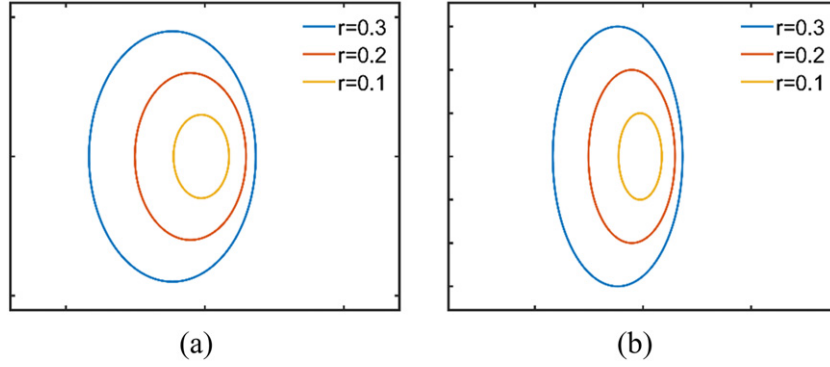


Figure 1. Cross-sections of equilibrium configuration for different elongations: (a) $\kappa = 1.5$; (b) $\kappa = 2$.

factors in the G–S equation. Thus, it is not feasible to obtain a pure radial force balance equation.

In the magnetic coordinates (r, θ_g, ζ_g) , equation (11) can be rewritten as

$$\begin{aligned} & \frac{\partial}{\partial r} \frac{J_g}{R^2} g^{rr} \frac{\partial \psi_p}{\partial r} + \frac{\partial}{\partial r} \frac{J_g}{R^2} g^{r\theta_g} \frac{\partial \psi_p}{\partial \theta_g} + \frac{\partial}{\partial \theta_g} \frac{J_g}{R^2} g^{\theta_g r} \frac{\partial \psi_p}{\partial r} \\ & + \frac{\partial}{\partial \theta_g} \frac{J_g}{R^2} g^{\theta_g \theta_g} \frac{\partial \psi_p}{\partial \theta_g} = \frac{J}{R^2} [-\mu_0 R^2 P'(\psi_p) - FF'(\psi_p)] \end{aligned} \quad (13)$$

where the geometric tensor coefficients can be found as:

$$g^{rr} = \frac{\kappa^2 \cos^2 \theta_g + \sin^2 \theta_g}{\kappa^2 (1 - \Delta' \cos \theta_g)}, g^{r\theta_g} = \frac{(-\kappa^2 + 1) \sin \theta_g \cos \theta_g - \Delta' \sin \theta_g}{\kappa^2 (1 - \Delta' \cos \theta_g)^2}, g^{\theta_g \theta_g} = \frac{\kappa^2 \sin^2 \theta_g + \cos^2 \theta_g}{\kappa^2 (1 - \Delta' \cos \theta_g)^2}. \quad (14)$$

$$\psi_p = \psi_0 + \psi_1(r - r_0) + \psi_2(r - r_0)^2 + \dots \quad (14)$$

Substituting equation (14) in the equation (13), we can obtain ψ_2 as

$$\begin{aligned} \psi_2 = & \frac{D^2}{2r^2 A} [-\mu_0 R^2 P'(\psi_p) - FF'(\psi_p)] - \frac{\partial}{\partial \theta_g} \left(\frac{C}{DR} \right) \\ & \times \frac{DR \psi_1}{2rA} - \frac{\partial}{\partial r} \left(\frac{r^2 A}{DR} \right) \times \frac{\psi_1 DR}{2r^2 A}, \end{aligned} \quad (15)$$

where the constants are defined as: $A = \kappa^2 \cos^2 \theta_g + \sin^2 \theta_g$, $D = \kappa r (1 - \Delta' \cos \theta_g)$, $C = (1 - \kappa^2) \sin \theta_g \cos \theta_g - \Delta' \sin \theta_g$, and the first order of the flux surface expansion is found to be $\psi_1 = \frac{\kappa B_0 r}{q}$.

Then we make the following choice: $\psi_p(r, \theta_g = 0) = \psi_p(r, \theta_g = \pi)$, which means, for a particular magnetic surface, the same radial coordinate ψ_p can be shifted horizontally to be tangent to this specific magnetic surface on both high and low field sides [34]. Then the relationship between Δ'' and α can be found by using the expansion in equation (15):

$$r(\Delta' + r)' = \frac{\alpha}{\kappa^2} \quad (16)$$

So far, we have finished adding elongation factor in the $s - \alpha$ equilibrium field model.

2.3. Geometric modifications with Boozer coordinates in ballooning space

Next we show the key geometric modifications to the gyrokinetic equation and vorticity equation when considering elongation in the equilibrium model. As is shown in equations (3) and (7), the Boozer coordinates are used for the gyrokinetic model and ballooning representation are used for the electromagnetic perturbations. The Boozer coordinate is not only a straight field line coordinate, but also satisfies $J_B = f(\psi_p)/B^2$. Equation (16) shows that the second order radial derivative of the Shafranov shift Δ , instead of Δ itself, is directly related to the elongation κ for fixed α , and in our equilibrium model, Δ is a negligible second order quantity. Therefore, accurate to $O(r)$, the Jacobian of the Boozer coordinates J_B can be obtained from equation (17)

$$J_B = (\nabla \psi_p \times \nabla \theta_B \cdot \nabla \zeta_B)^{-1} = \kappa r R_0 (1 + 2r \cos \theta_g) \quad (17)$$

Using this Boozer Jacobian, the relationship between the Boozer coordinates (r, θ_B, ζ_B) and magnetic coordinates (r, θ_g, ζ_g) used in the preceding section can be obtained:

$$\theta_B = \theta_g - (\Delta' + r) \sin \theta_g, \quad (18)$$

and

$$\zeta_B = \zeta_g - \nu(r, \theta_g) \quad (19)$$

where ν is a function of $O(r^2)$, which could be ignored in our model. In order to implement the shaping factor in the gyrokinetic equation and vorticity equation, we need to examine how the differential operators in these equations change with the shaping factor in the Boozer coordinates. The gradient operator in the Boozer coordinates can be written as $\nabla f = \nabla r \partial_r f + \nabla \theta_B \partial_{\theta_B} f + \nabla \zeta \partial_{\zeta} f$, which can be further expressed in the ballooning representation: [35]

$$\begin{aligned} \nabla f(r, \theta_B, \zeta) \rightarrow & [\nabla \theta (-inq + \partial_\theta) + \nabla r (-inq' \theta + \partial_r) \\ & + in \nabla \zeta] \hat{f}(\vartheta) \end{aligned} \quad (20)$$

With the preceding gradient operator and the equilibrium constraint in equation (16), and ignoring high order terms, we can find the quotient $\left(\frac{k_\perp}{k_\theta}\right)^2$ and magnetic drift term $\frac{\vec{B}}{B} \times \nabla$

In $B \cdot \mathbf{k}$ in the ballooning representation:

$$\kappa_{\perp}^2 = \left(\frac{k_{\perp}}{k_{\theta}}\right)^2 \rightarrow 1 + \left(s\theta - \frac{\alpha}{\kappa^2} \sin \theta\right)^2 + \frac{1 - \kappa^2}{\kappa^2} \left[\cos \theta + \left(s\theta - \frac{\alpha}{\kappa^2} \sin \theta\right) \sin \theta\right]^2 \quad (21)$$

$$\frac{\vec{B}}{B} \times \nabla \ln B \cdot \mathbf{k} \rightarrow \frac{k_{\theta} [\cos \theta + (s\theta - \frac{\alpha}{\kappa^2} \sin \theta) \sin \theta]}{\kappa} \quad (22)$$

$$P_{\parallel} = 1 \rightarrow \partial_{\parallel} = \frac{1}{qR} \partial_{\theta} \quad (23)$$

Using these expressions, the forms of g , κ_{\perp} and other relevant physical quantities in equations (3) and (7) can be calculated for the shaped plasma defined in equation (11) and implemented in the DAEPS code, as will be shown in next section.

3. DAEPS calculation of BAE instability with elongation

The coupling between SAWs and SW caused by the plasma compressibility could induce a gap for Alfvén continuum spectrum, where the BAE is located. Generally speaking, BAE can be excited either by thermal ions or by EPs through wave-particle resonance. In this paper, we focus our study on the BAE mode excited by the circulating thermal ions. The parallel mode structure of BAE is rather smooth, i.e., the BAE's mode structure in the ballooning representation changes slowly with the extended poloidal angle θ , which makes the ideal MHD assumption applicable, i.e., the parallel electric field $\delta E_{\parallel} \approx 0$.

The DAEPS code can calculate the BAE/KBM instability by invoking either a simple semi-analytic method or a more complex numerical method to integrate kinetic compression (KC) term: the simple method or reduced kinetic compression (rkC) method is based on a drift center transformation to integrate the KC term, which is fast computationally but less accurate; and the more complex method or complete kinetic compression (cKC) method is based on a brute force numerical integration of the KC term, namely the global h-adaptive multidimensional integration [25], which is more accurate but computationally much more expensive. Thus, the rkC method could be used not only to compute the linear eigenvalues in a semi-quantitative sense, but also to provide an initial guess for the eigen frequency ω , asymptotic behavior Λ , and help set up simulation domain and grid size for the cKC method. Moreover, the rkC method can also be used to analyze the physical mechanism because of its simplicity.

In the rkC method, the following drift center transformation is used to simplify the process of solving the gyrokinetic equation [14, 25, 36]. Firstly we make the following forward transformation to change the gyrocenter distribution δK_j to the drift center distribution δK_{dj} [36]:

$$\delta K_{dj} = \delta K_j \exp\left(\int^{\theta} i \frac{\omega_{dj}}{\omega_{ij}} d\theta\right) \quad (24)$$

Then the drift center distribution function δK_{dj} satisfies the following kinetic equation:

$$(\hat{\sigma}\omega_{ij}\partial_{\theta} - i\omega)\delta K_{dj} = i \frac{q_j}{m_j} QF_{0j} \frac{\Omega_{dj}}{\omega} J_0 \frac{g}{\kappa_{\perp}} \delta\Psi \times \exp\left(\int^{\theta} ik_{\perp}\rho_{dj} \frac{g}{\kappa_{\perp}} d\theta\right) \quad (25)$$

where $\rho_{dj} = qv/\omega_{ci}$, $\Omega_{dj} = \frac{\omega_{dj}}{g}$. As we have derived for shaped equilibrium, the geometric function g/κ_{\perp} in the preceding equation has the following form in the ballooning space:

$$\frac{g}{\kappa_{\perp}} = \frac{[\cos \theta + (s\theta - \frac{\alpha}{\kappa^2} \sin \theta) \sin \theta]}{\sqrt{1 + (s\theta - \frac{\alpha}{\kappa^2} \sin \theta)^2 + \frac{1 - \kappa^2}{\kappa^2} [\cos \theta + (s\theta - \frac{\alpha}{\kappa^2} \sin \theta) \sin \theta]^2}} \quad (26)$$

This expression is too complex to be integrated analytically over θ . However, in the inertial region ($\theta \gg 1$) where the kinetic response is non-negligible, the ballooning angle integration in equation (25) can be carried out approximately. Since $\frac{g}{\kappa_{\perp}}$ is an odd function of θ as $\theta \gg 1$, the expression in equation (26) can be expanded in the following Fourier series:

$$\frac{g}{\kappa_{\perp}} = G_1 \sin \theta + G_3 \sin 3\theta + \dots \quad (27)$$

where G_1 represents the first Fourier component in the poloidal angle expansion for the geodesic curvature coupled with the elongation effect. It is found that the G_1 term should be just sufficient to the requisite accuracy because G_1 is much larger than the rest expansion coefficients such as G_3 . And then it is calculated that G_1 takes the following form:

$$G_1 = \frac{1}{\pi} \int_0^{2\pi} \frac{\sin^2 \theta}{\sqrt{\kappa^2 \cos^2 \theta + \sin^2 \theta}} d\theta = \frac{2}{\pi(\kappa^2 - 1)} \left\{ \kappa^2 K(1 - \kappa^2) - E(1 - \kappa^2) + \kappa \left[K\left(1 - \frac{1}{\kappa^2}\right) - E\left(1 - \frac{1}{\kappa^2}\right) \right] \right\} \quad (28)$$

Therefore, the gyrokinetic equation for drift centre distribution becomes

$$(\hat{\sigma}\omega_{ij}\partial_{\theta} - i\omega)\delta K_{dj} = i \frac{q_j}{m_j} QF_{0j} \frac{\Omega_{dj}}{\omega} J_0 G_1 \sin \theta \delta\Psi \times \exp(-ik_{\perp}\rho_{dj} G_1 \cos \theta) \quad (29)$$

The exponential function in the preceding equation can be expanded in the Bessel series, $e^{ix \cos \theta} = \sum_n i^n J_n(x) e^{in\theta}$. In general, only the $n = 1$ term needs to be considered, thus the kinetic drift centre response can be found as

$$\delta K_{dj} = i \frac{q_j}{m_j} QF_{0j} \frac{\Omega_{dj}}{\omega} J_0 \delta\Psi \frac{J_1(G_1 k_{\perp} \rho_{dj})}{k_{\perp} \rho_{dj}} \left(\frac{e^{i\theta} - e^{-i\theta}}{\omega - \omega_{ij}} \right) \quad (30)$$

Use the pull-back transformation for the drift motion and insert the preceding expression in equation (7), we can obtain the following form for the kinetic compression:

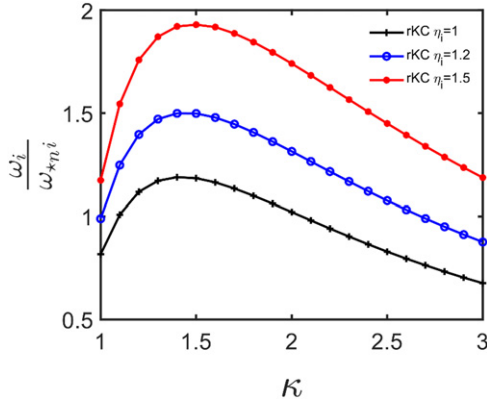


Figure 2. Linear growth rate or $\text{Im } \Omega = \omega_i/\omega_{*mi}$ of BAE instability varies with elongation factor κ for various η_i .

$$\text{KC} = \left\langle \frac{4\pi q_j^2 q^2 R^2}{k_\theta^2 c^2 m_j} Q F_j \Omega_{dj}^2 \delta \Psi \times \frac{J_{0r}^2 J_1^2(G_1 k_\perp \rho_{di})}{(k_\perp \rho_{di})^2} \left(\frac{e^{2i\theta} + e^{-2i\theta} - 2}{\omega - \omega_{ii}} \right) \right\rangle. \quad (31)$$

In equation (31), ω_{ii} is the ion transit frequency $\frac{|v_{ii}|}{qR}$, with $v_{ii} = \sqrt{\frac{2T_i}{m_i}}$, and the $J_n(k_\perp \rho_j)$ is the n th order Bessel function of the first kind. In the long wavelength limit, we can obtain:

$$\text{KC} = \left\langle \frac{4\pi q_j^2 q^2 R^2}{k_\theta^2 c^2 m_j} Q F_j \Omega_{dj}^2 \delta \Psi \frac{1}{\omega - \omega_{ii}} G_1^2 \sin^2 \theta \right\rangle. \quad (32)$$

According to the theory [20], both BAE and KBM can be driven by η_i . Below some critical value of η_{ic} , the KBM is the most unstable mode; and above η_{ic} , the KBM is coupled with the BAE mode. The traditional calculation of the BAE/KBM instability by the DAEPS code is based on the concircular flux surface model [25]. Here we show how the BAE/KBM growth rate varies with elongation of the magnetic flux surface, as is shown in figure 2, where the data is calculated by the DAEPS code with plasma parameters $\beta_i = 0.01$, $k_\theta \rho_i = 0.19$, $s = 0.2$, $q = 1.5$, $\omega_{*mi} = \omega_{Ti}$, and $\eta_i = 1, 1.2, 1.5$.

As can be seen from figure 2, the growth rate or $\text{Im}(\Omega)$ with $\Omega \equiv \omega/\omega_{*mi}$ of the BAE mode firstly increases with elongation to a maximum value as the elongation $\kappa \sim 1.5$, and then it decreases with the elongation monotonically. In this case, we note that the pressure gradient α increases with η_i , e.g., $\alpha = 0.45, 0.495, 0.5625$ when $\eta_i = 1, 1.2, 1.5$, respectively. Figure 2 also shows that, for the same elongation κ , the growth rate $\text{Im } \Omega$ increases with η_i and thus increases with α , which is consistent with the BAE theory [20, 25].

Figure 3 exhibits parallel mode structures of BAE for $\kappa = 3$ and $\eta_i = 1$ using reduced integration method for the kinetic compression (KC) term. The mode structure is symmetric in θ according to the symmetry of KC term, which is due to the strong destabilizing effect of bad curvature on the outboard middle plane. This rKC method is semi-analytic and much faster than the brute force integration method or cKC method, which are both implemented in the DAEPS code. The DAEPS

code requires that the simulation domain should be wide enough to cover the non-vanishing asymptotic mode structure for the outgoing wave boundary condition, and the grid size should be small enough to achieve numerical convergence, e.g., $\Delta\theta < 0.2$. It can be seen from figure 3(a) that the widths of different mode structures are in the range of $[-50, 50]$, which is much narrower than the simulation domain. The fast-spatial oscillation component of the mode in figure 3(a) is caused by $P(\theta)$, which is an oscillatory function with a period of 2π . According to the Floquet theory and equation (5), the logarithm of Ψ varies linearly with the ballooning angle θ in the inertial region, which suggests that there is negligible numerical error generated by the numerical asymptotic matching process. Thus, the mode structure in the ideal region can hardly be distorted by the inertial region computation. Using this asymptotic matching process for the boundary condition, we can significantly narrow down the simulation domain in the inertial region while maintaining high computational accuracy. For example, the simulation domain is set as $[-100, 100]$ for the calculation in figure 3(a), and the grid size is set as $\Delta\theta = 0.05\pi$. With these settings, we can use cKC method to calculate the eigen frequency for the BAE mode.

With the parallel mode structure of BAE in the ballooning representation, a demonstration of two-dimensional mode structure could be made in real space using the following transform:

$$\delta\psi(r, \theta, \zeta) = \sum_{n,m} e^{i(n\zeta - m\theta)} \int e^{-i(nq - m)\theta'} \delta\psi_n(r, \theta') d\theta', \quad (33)$$

where θ' is the ballooning angle and θ is the angle in the real space. The mode structure so far computed is local and 1D in parallel. In order to mimic the global radial variance, we choose $n = 4, m = 6$, and $q = 1.5$ and modulate the mode function artificially with an envelope function $M(r)$, i.e., a super Gaussian function, defined by the following form:

$$M(r) = \exp\left[-\frac{(r - r_c)^4}{\Delta r^4}\right], \quad (34)$$

where we choose $r_c = a/2$, $\Delta r = a/2$. The resultant two-dimensional mode structure is illustrated in figure 4, which is similar to the 2D mode structure calculated by other simulation codes [19], except the elongation effect.

4. Theoretical analysis for elongation effect on BAE

In this section, we provide detailed theoretical analysis for the elongation effect on the BAE instability. First we show how the BAE growth rates varies with elongation κ using the DAEPS code, as is demonstrated in figure 5, where the result from the rKC method is compared to the completed KC term (cKC) method, with the same parameters as in the $\eta_i = 1$ case in figure 2. The red circle line is the growth rate $\text{Im } \Omega$ calculated by cKC while the blue plus line is the growth rate or $\text{Im } \Omega$ calculated by reduced KC term (rKC). The growth rate from rKC agrees well quantitatively with that from cKC, justifying the use of the simplification method of rKC. This agreement

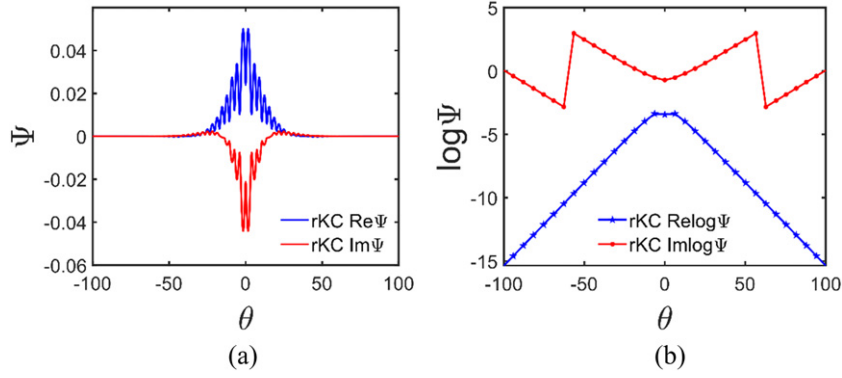


Figure 3. BAE mode structure for elongated equilibrium with $\kappa = 3$ and $\eta_i = 1$ using rKC integration method for the KC term. (a) Linear scale; (b) logarithmic scale.

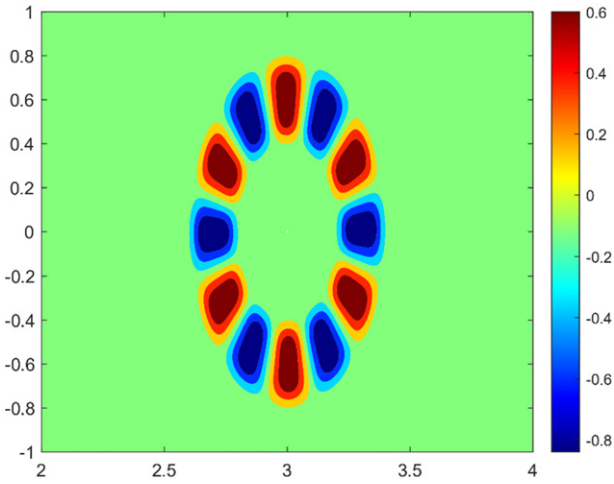


Figure 4. 2D mode structure of BAE in poloidal plane with $\kappa = 2$.

provides a solid basis for investigating the instability BAE using the formula in equation (32).

As is shown in figure 5(a), the growth rate of BAE firstly increases with the elongation κ , reaches a maximum, and then decreases. In order to analyze kinetic and fluid/MHD contributions to the growth rate of BAE/KBM, we artificially remove the kinetic compression term and recalculate the growth rate. As is shown in figure 5(b), the red circle line is obtained from the cKC method, the blue plus line is obtained by removing the KC term, and the black diamond line is calculated without the FLR and FOW effect. The trend of growth rate varying with κ without the kinetic compression term (KC) or δW_k is essentially the same as the original trend. And there exists a notable difference between the growth rates with and without the KC term when the elongation $\kappa > 2.5$. In this strongly elongated region, the BAE growth rate with only the MHD effect decreases rapidly with κ increasing, and it nearly disappears at $\kappa = 3$. However, the stability results with the KC term shows that the BAE is still unstable, and decreases gradually around $\kappa = 3$. Based on these observations, it is then conjectured that the trend of the BAE instability is mainly related to the MHD effect around the turning point ($\kappa \approx 1.5$),

and the instability in the strongly elongated region $\kappa > 2.5$ is caused by the kinetic effect, such as wave–particle resonance.

To justify our viewpoint, the kinetic contribution to the potential energy δW_k , and the fluid contribution to the potential energy δW_f needs to be examined as κ increases. δW_k can be calculated by $\langle \delta\psi | \text{KC} | \delta\psi \rangle$, where $\delta\psi$ is the normalized eigenfunctions, and δW_f can be acquired by $\langle \delta\psi | W | \delta\psi \rangle$, where W contains the Schrödinger potential well term (interchange term) and field line bending term. Therefore, we could rewrite the vorticity equation as

$$C\omega + D\omega^2 - i\Lambda B - \delta W_f - \delta W_k = 0 \quad (35)$$

Similarly, $C = \langle \delta\psi | \frac{-\omega_{*pi}}{\omega_A^2} | \delta\psi \rangle$, $D = \langle \delta\psi | \frac{1}{\omega_A^2} | \delta\psi \rangle$, and $B = \langle \delta\psi | B \cdot C \cdot | \delta\psi \rangle$ is the boundary condition term, which is much smaller than δW_f and δW_k for this case. Thus equation (35) is a quadratic equation about ω and its solution can be expressed as

$$\omega = \frac{-C/2 \pm \sqrt{\frac{C^2}{4} + D(\delta W_f + \delta W_k)}}{D} \quad (36)$$

To verify the previous conjecture, we could solve the preceding eigen equation by ignoring $\text{Im} \delta W_k$, and compare the resultant eigenvalue ω . As is shown in figure 6(a), the trend of the growth rate is almost the same in both cases when $\kappa < 2$, which suggests a fluid instability of reactive type. But in the region $\kappa > 2.5$, there is a noticeable difference: when the whole kinetic compression term is considered, the growth rate decreases gradually with κ ; whereas when $\text{Im} \delta W_k$ is ignored, the growth rate decays rapidly. Therefore, $\text{Im} \delta W_k$ is the main cause of the instability of BAE in this strongly elongated region. We proceed to verify our previous conjecture by analyzing the change in the magnitude of various potential energies in figure 6(b). When $1 < \kappa < 2$, the change of δW_k can be considered to be approximately invariant compared to δW_f . Thus, in this region, the change in the growth rate is mainly determined by the change in δW_f . When $\kappa > 2.5$, both δW_f and $\text{Re} \delta W_k$ decays towards zero and they tend to cancel each other. In fact, in this region, $\delta W_f + \text{Re} \delta W_k$ can be shown to be much smaller than $\text{Im} \delta W_k$ in figure 6(b). This suggests that the instability or linear growth is mainly caused by $\text{Im} \delta W_k$ in this region.

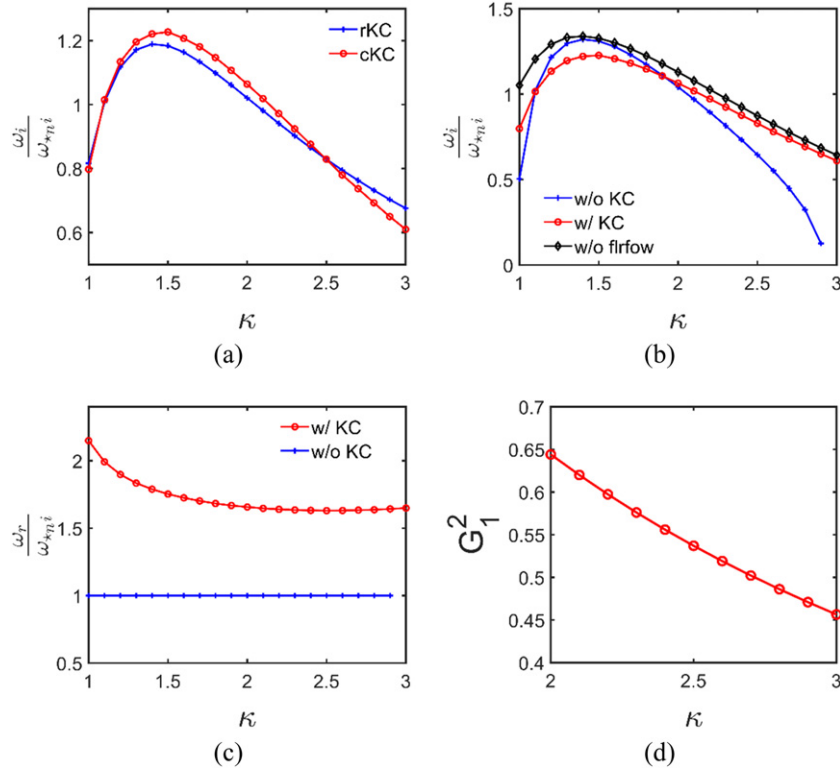


Figure 5. (a) Comparison of BAE growth rate with rKC term and cKC term for $\eta_i = 1$. (b) The growth rate of BAE ignoring different parts of kinetic compression term for $\eta_i = 1$. (c) The real frequency of BAE with and without kinetic compression term for $\eta_i = 1$. (d) The first order poloidal Fourier coefficient G_1 decreases with κ increasing from 2.5 to 3.

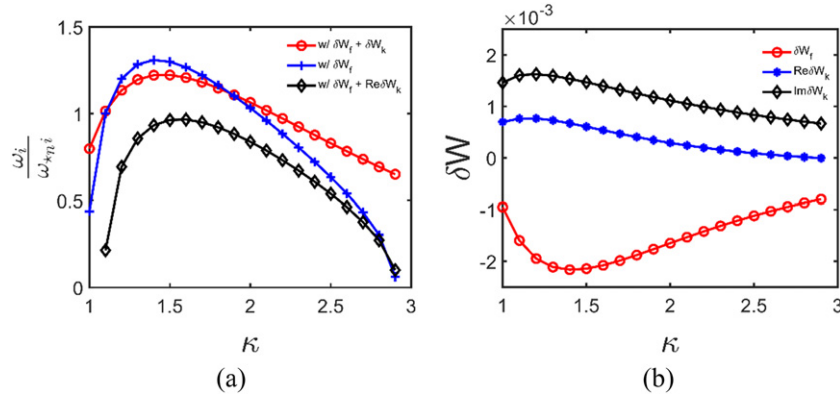


Figure 6. (a) Growth rate varies with elongation factor κ with different forms of KC term. (b) The local kinetic and fluid contribution to potential energy as κ increases.

As figure 5(b) shows, the kinetic contribution δW_k decreases with elongation κ when $\kappa > 2.5$. The red circle and black diamond lines in figure 5(b) represents BAE growth rates vs κ with or without FLR-FOW (finite Larmor radius & finite orbit width) effects respectively. These two lines are coincident with each other when $\kappa > 2.5$, which suggests that the FLR or FOW effect has little influence on the growth rate. Therefore, the kinetic effect in this region is mostly likely due to wave-particle resonance, which corresponds to $\text{Im} \delta W_k$ mathematically and suggests a dissipative instability. Note that we here focus on the trend of the BAE's growth rate changing with elongation. The effect of FLR and FOW on the growth

rate for κ close to unity is significant, but this effect becomes minimal when κ increases and the trend of the BAE's growth rate varying with elongation does not change with including FLR and FOW.

Next we try to analyze why the wave-particle resonance effect decays with elongation κ increasing in the strongly shaped region. We examine the form of kinetic compression term with holding off the FLR and FOW effects after performing the drift center transformation. As equation (36) shows, the kinetic compression term is related to $\frac{1}{\omega - \omega_{ij}}$, i.e., the wave-particle resonance kernel, and the first order Fourier coefficients G_1 while the first-order expansion is dominant as

shown in figure 5(a). When $2.5 < \kappa < 3$, the real frequency ω_r is almost constant in figure 5(c), suggesting that the resonance position is almost unchanged in this region. Figure 5(d) shows that G_1 decreases with the elongation κ , which means the first poloidal Fourier coefficient of $\frac{g}{\kappa_\perp}$ decreases with κ . Thus, according to figure 5(d) and equation (32), we can find that the decrease in δW_k is mainly caused by the decrease in G_1 , which contains all the elongation effect in the KC term. The decrease in the kinetic compression in the dissipative region is due to the decrease in the projection of geodesic curvature on the poloidal direction rather than the shift in the wave particle resonance point.

5. Conclusion and discussion

In this paper, we have constructed a local $s - \alpha$ equilibrium model including the elongation factor and implemented this model in the DAEPS code by modifying the gyrokinetic equation and vorticity equation using the Boozer coordinates and ballooning representation. The elongation effect on the BAE caused by the thermal ions has been investigated by the DAEPS code with thermal ions as the kinetic compression. In order to calculate the growth rate of BAE/KBM accurately and quickly, we have also upgraded the rKC. The elongation factor has been included in the vorticity equation including the KC term for both cKC and rKC method. It is discovered that the BAE growth rate first increases, reaches a maximum and then decreases with elongation. This trend occurs for many different values of η_i and quite general. We find that, when the shape of cross-section is close to circular, e.g., $1 < \kappa < 2$, the trend of growth rate is mainly determined by the fluid/MHD effects, namely the combination of the field line bending term and potential well term in the vorticity equation, which suggests a reactive instability. However, for strongly shaped plasma with $\kappa > 2.5$, the growth rate is mainly driven by the wave-particle resonance embedded in δW_k , which suggests a dissipative instability. In this dissipative region, the wave-particle resonance effect decreases with the elongation κ since the dominant poloidal Fourier component of the geodesic curvature decreases with elongation while the resonant point keeps unchanged. The physics conclusion in this paper is pretty general for the long wavelength modes with $k_\perp \rho_i < 1$, which is more relevant for most turbulence observed in experiments. However, for short wavelength modes, the stabilizing effect of the diamagnetic flow becomes more prominent and the fluid instability is hard to excite. Then the physics scenario discovered in this study may no long occur.

As has been demonstrated, the plasmas shaping effects such as elongation can introduce many interesting physics phenomena in the drift-Alfvénic instability such as BAE. Our results further suggest that the non-monotonic feature of the BAE growth rate varying with elongation would have important consequences on the nonlinear transport of BAE turbulence, since as is shown in reference [22], the saturation magnitude of BAE turbulence is determined by the linear growth rate in the small phase island case. In the future, we will introduce more shaping factors in our calculation, e.g., the triangularity,

to investigate how these shaping factors influence various drift-Alfvénic instabilities and turbulences.

Acknowledgments

One of the authors, Yong Xiao, thanks helpful discussions with Professor Liu Chen and Professor Zhihong Lin. This work is supported by National MCF Energy R & D Program of China under Grant No. 2019YFE03060000, and by NSFC under Grant No. 11975201.

ORCID iDs

Yong Xiao  <https://orcid.org/0000-0001-5333-2867>

References

- [1] Cheng C., Chen L. and Chance M. 1985 High- n ideal and resistive shear Alfvén waves in tokamaks *Ann. Phys., NY* **161** 21–47
- [2] Cheng C.Z. and Chance M.S. 1986 Low- n shear Alfvén spectra in axisymmetric toroidal plasmas *Phys. Fluids* **29** 3695
- [3] Fu G.Y. and Van Dam J.W. 1989 Excitation of the toroidicity-induced shear Alfvén eigenmode by fusion alpha particles in an ignited tokamak *Phys. Fluids B* **1** 1949–52
- [4] Chen Y., Parker S.E., Lang J. and Fu G.-Y. 2010 Linear gyrokinetic simulation of high- n toroidal Alfvén eigenmodes in a burning plasma *Phys. Plasmas* **17** 102504
- [5] Rizvi H., Ryu C.M. and Lin Z. 2016 Multiple toroidal Alfvén eigenmodes with a single toroidal mode number in KSTAR plasmas *Nucl. Fusion* **56** 112016
- [6] Wang X., Zonca F. and Chen L. 2010 Theory and simulation of discrete kinetic beta induced Alfvén eigenmode in tokamak plasmas *Plasma Phys. Control. Fusion* **52** 115005
- [7] Heidbrink W.W. et al 2021 Isotope dependence of beta-induced Alfvén eigenmode (BAE) and low frequency mode (LFM) stability in DIII-D *Nucl. Fusion* **61** 106021
- [8] Chu M.S., Greene J.M., Lao L.L., Turnbull A.D. and Chance M.S. 1992 A numerical study of the high- n shear Alfvén spectrum gap and the high- n gap mode *Phys. Fluids B* **4** 3713–21
- [9] Heidbrink W.W., van Zeeland M.A., Austin M.E., Crocker N.A., Du X.D., McKee G.R. and Spong D.A. 2021 Stability of beta-induced Alfvén eigenmodes (BAE) in DIII-D *Nucl. Fusion* **61** 066031
- [10] Chen W. et al 2010 β -induced Alfvén eigenmodes destabilized by energetic electrons in a tokamak plasma *Phys. Rev. Lett.* **105** 185004
- [11] Lauber P. et al 2012 NBI-driven Alfvénic modes at ASDEX Upgrade *Nucl. Fusion* **52** 094007
- [12] Lauber P. et al 2009 Kinetic Alfvén eigenmodes at ASDEX Upgrade *Plasma Phys. Control. Fusion* **51** 124009
- [13] Chen L. 1994 Theory of magnetohydrodynamic instabilities excited by energetic particles in tokamaks *AIP Conf. Proc.* **311** 63
- [14] Chen L. and Zonca F. 2016 Physics of Alfvén waves and energetic particles in burning plasmas *Rev. Mod. Phys.* **88** 015008
- [15] Wang S. 2001 Destabilization of internal kink modes at high frequency by energetic circulating ions *Phys. Rev. Lett.* **86** 5286–8
- [16] Van Zeeland M.A. et al 2019 Alfvén eigenmodes and fast ion transport in negative triangularity DIII-D plasmas *Nucl. Fusion* **59** 086028

- [17] Kusama Y. *et al* 1998 Toroidal Alfvén eigenmodes driven with ICRF accelerated protons in JT-60U negative shear discharges *Nucl. Fusion* **38** 1215–23
- [18] Heidbrink W.W., Ruskov E., Carolipio E.M., Fang J., van Zeeland M.A. and James R.A. 1999 What is the ‘beta-induced Alfvén eigenmode?’ *Phys. Plasmas* **6** 1147–61
- [19] Zhang H.S., Lin Z., Holod I., Wang X., Xiao Y. and Zhang W.L. 2010 Gyrokinetic particle simulation of beta-induced Alfvén eigenmode *Phys. Plasmas* **17** 112505
- [20] Zonca F., Chen L. and Santoro R.A. 1996 Kinetic theory of low-frequency Alfvén modes in tokamaks *Plasma Phys. Control. Fusion* **38** 2011–28
- [21] Briguglio S., Vlad G., Zonca F. and Kar C. 1995 Hybrid magnetohydrodynamic-gyrokinetic simulation of toroidal Alfvén modes *Phys. Plasmas* **2** 3711–23
- [22] Todo Y. and Sato T. 1998 Linear and nonlinear particle-magnetohydrodynamic simulations of the toroidal Alfvén eigenmode *Phys. Plasmas* **5** 1321–7
- [23] Zhu J., Ma Z.W. and Wang S. 2016 Hybrid simulations of Alfvén modes driven by energetic particles *Phys. Plasmas* **23** 122506
- [24] Zhang H.S., Lin Z. and Holod I. 2012 Nonlinear frequency oscillation of Alfvén eigenmodes in fusion plasmas *Phys. Rev. Lett.* **109** 025001
- [25] Li Y., Hu S., Zheng W. and Xiao Y. 2020 Drift Alfvén energetic particle stability with circulating particles *Phys. Plasmas* **27** 062505
- [26] Qi L., Dong J.Q., Bierwage A., Lu G. and Sheng Z.M. 2013 Thermal ion effects on kinetic beta-induced Alfvén eigenmodes excited by energetic ions *Phys. Plasmas* **20** 032505
- [27] Xie H.-S., Lu Z.-X. and Li B. 2018 Kinetic ballooning mode under steep gradient: high order eigenstates and mode structure parity transition *Phys. Plasmas* **25** 072106
- [28] Gao Z., Wang P. and Sanuki H. 2008 Plasma shaping effects on the geodesic acoustic mode in toroidally axisymmetric plasmas *Phys. Plasmas* **15** 074502
- [29] Qi L., Kwon J., Hahm T.S. and Jo G. 2016 Gyrokinetic simulations of electrostatic microinstabilities with bounce-averaged kinetic electrons for shaped tokamak plasmas *Phys. Plasmas* **23** 062513
- [30] Miller R.L., Chu M.S., Greene J.M., Lin-Liu Y.R. and Waltz R.E. 1998 Noncircular, finite aspect ratio, local equilibrium model *Phys. Plasmas* **5** 973–8
- [31] Zonca F. and Chen L. 2014 Theory on excitations of drift Alfvén waves by energetic particles: I. Variational formulation *Phys. Plasmas* **21** 072120
- [32] Zonca F. and Chen L. 2014 Theory on excitations of drift Alfvén waves by energetic particles: II. The general fishbone-like dispersion relation *Phys. Plasmas* **21** 072121
- [33] Freidberg J.P. 2014 *Ideal MHD* (Cambridge: Cambridge University Press)
- [34] Yu W., Zhou D. and Xiang N. 2012 A novel local equilibrium model for shaped tokamak plasmas *Phys. Plasmas* **19** 072520
- [35] Connor J.W., Hastie R.J. and Taylor J.B. 1978 Shear, periodicity, and plasma ballooning modes *Phys. Rev. Lett.* **40** 396–9
- [36] Tsai S. and Chen L. 1993 Theory of kinetic ballooning modes excited by energetic particles in tokamaks *Phys. Fluids B* **5** 3284